Chiral polymeric nanocapsules and their use for conformational deracemization of liquid crystals

Amani Zoabi[a], Melvin G. Santiago[b, ^], Dmitri Gelman[a], Charles Rosenblatt[a,b*], David Avnir[a,c] and Raed Abu-Reziq[a,c*]

[a] Institute of Chemistry and [c] the H. M. Kruger Center for Nanoscience and Nanotechnology, the Hebrew University of Jerusalem, Jerusalem, 9190402, Israel, and [b] Department of Physics, Case Western Reserve University, Cleveland, Ohio 44106, USA

Abstract

We present the first preparation and properties of chiral nanocapsules. The chiral shell, a polyurea derivative, was obtained by interfacial emulsion polymerization of L-lysine with polymethylene polyphenyl isocyanate. The chirality of these nanocapsules was manifested by its ability to induce conformational deracemization of liquid crystal. This induced chirality was measured using the "Raynes experiment", in which the cell's boundary conditions impose a $\pm 90^{o}$ rotation of the liquid crystal director from one surface to the other. Both left and right-handed director twist domains appear on cooling from the isotropic to the nematic phase. Owing to the weak induced chirality of the liquid crystal, one sense of director rotation is energetically more favorable and its domain size expands, resulting in curvature of the domain walls. The curvature was measured as a function of capsule concentration, and serves as a metric of the induction of chirality in the surrounding liquid crystal.

^ Present address: Department of Physics, Ohio State University, Columbus, Ohio, USA

Introduction

Because of the significance of chiral molecules in numerous biochemical and medical applications,[1] great effort has been devoted to developing methods for the enantioselective synthesis, separation and isolation of these molecules, as well as for the characterization of their ability to induce chirality in a surrounding media such as liquid crystals.[2-5] Surface solid state methods have been particularly central in these efforts due to their ability to affect enantioselective adsorptions, separations, and catalysis[6-15]. Importantly, in the arsenal of chiral materials and interfaces, the use of *polymeric nanocapsules having a chiral shell* is not known, despite the fact that physical and chemical methods for the preparation of achiral polymeric capsules exist[16-19]. Here we report the successful synthesis of chiral polyurea nanocapsules by interfacial [20-22] cross-linking reaction of polymethylene polyphenyl isocyanate with L-lysine in a nanoemulsion. We further report the first demonstration of the ability of chiral nanocapsules to induce chirality within a liquid crystal phase. Such chiral inductions are of great interest because they facilitate control of electrooptic switching and photonic bandgap devices, biological and chemical sensors, and provide a means for testing optical purity of pharmaceuticals.[23-33] For that purpose we have chosen a configurationally achiral but conformationally racemic liquid crystal 4-cyano-4'-pentylbiphenyl (5CB) as the external matrix owing to its high susceptibility for deracemization and favorable optical and mechanical properties. The shells were suspended in the liquid crystal host, and we measured the chirality induced in the liquid crystal by exploiting its ability to conformationally deracemize and thereby induce a helical twist of the nematic director. Nearly a century ago Friedel showed that the addition of chiral dopants to a nematic phase induces a helical twist of the director.[34] Theoretically, in the so-called surface chirality model[35,36], each element of the dopant's molecular surface experiences a mean field due to the surrounding nematic host. The host interaction potential with the dopant changes accordingly. Because typical nematic

molecules with flexible cores can thermally interconvert between *R*- and *S*-conformations, a chiral dopant stabilizes the appropriate chiral conformation of the host liquid crystal.[35,37] In this manner chirality is transferred from the dopant to the nearest neighbor LC host molecule, then to the next-nearest-neighbor, and so on, resulting in a deracemization of the nematic host near the chiral dopant and a net twist of the nematic director.

Experimental Details

Chemicals: Polymethylene polyphenyl isocyanate (PAPI 27), poly(1-ethenyl pyrrolidin-2-one/hexadec1-ene) (Agrimer Al 22) and Reax 88b were contributed by FMC Corporation. Ethyl cinnamate, sodium dodecyl sulfate (SDS) and L-lysine monohydrochloride were purchased from Sigma-Aldrich. 4-Cyano-4'-pentylbiphenyl (5CB) was obtained from Frinton Laboratories. Polyamic acid PI2555 was purchased from DuPont.

Synthesis of the chiral polyurea nanocapsules: An oil phase containing 16.8 g ethyl cinnamate and 3.2 g of PAPI 27 was nanoemulsified with 63 g water containing 2 g of the surfactant sodium dodecyl sulfate (SDS) by sonication for 45 minutes which was carried out using Sonics Vibra-Cell VCX 130 Ultrasonic Cell Disruptor with an output of 130 W and 20 kHz. The resulting nanoemulsion was heated at 35 °C for 5 minutes followed by adding 2.5 g of L-lysine monohydrochloride dissolved in 15 g water. After stirring for 30 minutes the temperature was raised to 55 °C and stirring continued for 24 hours. The resulting chiral nanocapsules were separated by ultracentrifugation at 13000 rpm and washed three times with water.

Nanocapsules characterizations: Images were acquired using a high resolution scanning electron microscope (HR SEM), Sirion (FEI Company), using a Schottky type field emission source and a secondary electron (SE) detector. The images were scanned at 5 kV acceleration voltages. SEM with focused ion beam (FIB) and optical microscopy was performed with FEI Helios NanoLab 460F1 DualBeam (ThermoFidher Scientific). Transmission electron microscopy (TEM) was performed with a (S) Tecnai F20

G2 (FEI company) operated at 200 kV. Cryogenic transmission electron microscopy (cryo-TEM) was performed at -177ºC using FEI Tecnai 12 G2 TWIN TEM operated at 120 kV and equipped with a Gatan model 626 cold stage. Dynamic light scattering measurements (DLS) were performed using the Malvern Zetasizer Nano, model ZEN3600. The IR spectra were recorded at room temperature in transmission mode on a Perkin Elmer 65 FTIR spectrometer. Sonication was carried out using Sonics Vibra-Cell VCX 130 Ultrasonic Cell Disruptor with an output of 130 W and 20 kHz. Circular dichroism (CD) measurements were performed by MOS-500 Spectrometer (BioLogic Science Instruments).

Deracemization experiments and measurements by Raynes' method: The doping concentration range of the chiral nanocapsules — ~ 0.1 to 0.5 wt-% — was chosen based on preliminary examination of samples ranging up to about 1.5 wt-%. The nanocapsules remain most dispersed at the lowest concentrations, with aggregation increasing continuously with increasing concentration. At concentrations above 0.5 wt-%, the samples showed an intolerably high degree of aggregation of capsules. This would become a confounding factor in the data analysis, as the surface-to-volume ratio of the capsules would be reduced compared to that of the individual capsules, thus reducing the deracemization effect. Therefore, we limited the upper range of capsule concentration to ~ 0.5 wt-%, keeping in mind that there is some aggregation at all nonzero concentrations, which becomes worse as the concentration increases. The desired amount of capsules was added to toluene and sonicated for 20 min. The capsule/toluene mixture was in turn added to the 5CB LC with additional toluene to reach final concentrations of 0, 0.11, 0.21, 0.32, 0.42, and 0.52 wt-% of capsules. Cells were created by cleaning microscope slides (2.5 x 2.5 cm) in detergent, acetone, and ethanol, then spin coating with the polyamic acid PI2555 (DuPont) for 2 s at 400 rpm and then for 40 s at 3600 rpm. The slides subsequently were baked at 80^{o} C for 30 min and then further baked at 250^{o} C for 60 min. The resulting polyimide layers were then rubbed unidirectionally with a commercial rubbing cloth to create an "easy axis" direction for alignment of the LC molecules on each substrate. One of the coated slides was coated with a very small number, approximately 100 per mm^2 of substrate surface area, of 10 μm diameter polymer spacer rods. The other coated slide was placed on top

with its easy axis direction rotated by 90^{o} with respect to the first substrate, and the two slides held together mechanically by clips. Similar cells were prepared for each concentration of capsule/LC mixture. The cells were filled by capillary action in the isotropic phase of the liquid crystal at ~ 37^{o} C and cooled to room temperature, which is in the LC nematic phase. The cells were photographed ~18 h after they were removed from the oven. Cells were placed under a polarizing optical microscope with polarizers rotated to maximize the contrast of the domain walls. Images were taken using a 20x objective with a 2784 x 1856 pixel CCD camera then converted to a greyscale bitmap file using Image-J® software. With this image size, the pixel-to-length conversion factor was 0.63 micrometers per pixel. MatLab® was used with a Canny routine[38] to locate and digitize the domain walls, after which the walls were fitted to the arc of a circle using a least-squares method to determine the local radius of curvature *r*.

Results and discussion

The chiral nanocapsules: As discussed in the Introduction, chiral-shell nanocapsules are not known. This type of capsules was prepared by dissolving polymethylene polyphenyl isocyanate in ethyl cinnamate and nanoemulsifying the resulting solution in water containing the surfactant sodium dodecyl sulfate (SDS) by sonication for 45 minutes. Upon addition of L-lysine to the nanoemulsion, an interfacial polyaddition reaction took place (Scheme 1), resulting in the chiral polyurea nanocapsules with an average size of 176 ±5 nm and shell thickness of 7 nm, as revealed by TEM and cryo-TEM imaging (Fig. 1). The hollow nature of these capsules is also revealed by their collapse under the high vaccum SEM conditions. It is important to note that the capsules remain mostly spherical when dissolved in the liquid crystal. In addition, SEM after dissection with focused ion beam (FIB) showed core-shell structure. (Fig. 2). The chirality of the shell and the successful incorporation of the L-lysine within it were confirmed by CD spectroscopy with a typical signal at 212 nm (Fig. 3a). Further structural confirmation is provided by infrared (IR) analysis (Fig. 3b) which shows the stretching of the N-H at 3346 cm^{-1} and the stretching of the C=O of the urea groups at 1656 cm^{-1}, along with the absence of the characteristic absorption peak of the isocyanate groups of polymethylene polyphenyl isocyanate at 2250-2270 cm^{-1}, all of which clearly indicate the formation of the polyurea shell. ^{13}C CP-MAS NMR

spectroscopy (Fig. 3c) clearly show the methylene groups of the L-lysine units at 13-39 ppm, the methylene groups attached to the aromatic rings as well as the methyl groups of the ethyl cinnamate, the methine groups of the L-lysine at 55 ppm, the methylene groups of the ethyl cinnamate peaks at 60 ppm, the aromatic and olefinic carbon atoms at 118-157, the carbonyl group of the urea at 156 ppm, the carbonyl group of ethyl cinnamate at 167, and the carbon of the carboxylic acid group of the L-lysine at 179 ppm.

The liquid-crystals conformational deracemization measurements: We demonstrate the chiral nature of the nanocapsules by their ability to induce de-racemization in conformationally racemic LC domains; the interest in that process has been summarized in the introduction. The deracemization is detected using the Raynes technique,[39] which is extremely sensitive to the very long helical pitches (>> cell thicknesses, which are of order a few μm) associated with weak chiral induction. Techniques for measuring pitches of order a few micrometers, such as the Cano wedge or the fingerprint method, are not applicable here,[40] as our induced helical pitches are several hundred micrometers. The Raynes' method uses a twist cell in which the "easy axes" for LC alignment at the two surfaces are rotated by 90^{o}. The director of an achiral LC would undergo an approximately $\pm 90^{o}$ rotation from one surface to the other, nucleating as left-handed helices and right-handed helices with equal probability. Specifically, one begins with an achiral — actually conformationally racemic — LC. By imposing that 90^{o} boundary surfaces rotation, the director of the LC will helically twist from one interface to the other forming either left- or right-handed helical domains with equal probability. The handedness of the domain will depend on which twist-handedness of the LC molecule (left twist or right twist around the biaryl bond of the 5CB molecule) nucleates the local supramolecular build-up of the nematic phase upon cooling from the isotropic phase. As these nucleated domains grow, they will eventually meet — with straight walls separating these domains. We note that the helical quarter-pitch axis is oriented perpendicular to the cell plane – this is the so-called Grandjean orientation[40] – and thus no texture should be visible other than these domain walls. This racemic distribution of domains may change upon introduction of a chiral dopant if that dopant has some interaction (hydrogen bonds, pi-pi bonds, van der Vaals interactions, etc.) with

the LC molecule. In that case, deracemization of the domains may occur because of the different diastereomeric interactions between the chiral dopant – say left handed as in our case – and each of the two enantiomeric twists of the LC molecule: Preference in the nucleation for one of the two possible nematic helices will occur. In the Raynes experiment this manifests in the conversion of the straight boundary lines between the domains – which tend to be pinned at the spacer rods or at other particulates — into curved boundary lines, where the preferred helical enantiomer domains push into the less favorable opposite enantiomer domains. In the approximation that the splay, twist, and bend elastic constants are equal, Raynes showed that the chiral dopant induced pitch of the liquid crystal $P = 2r$, where r is the radius of curvature of the domain wall. Thus, mixing the chiral capsules into a liquid crystal facilitates a demonstration of chiral induction by a measurement of the average curvature C (defined as $\langle 1/r \rangle$) as a function of the concentration x of the chiral capsules.

The LC host we used - 4-cyano-4'-pentylbiphenyl (5CB**,** Scheme 1) is composed of a racemic mixture of chiral conformers, of which the relevant for our discussion are the left/right handed rotamers of the biphenyl moiety. As the substituents of the biphenyl unit are in the *para* position, the barrier for rotation is low, ~ 3.5 kJ mol^{-1}. The pentyl tail contributes to the library of possible chiral conformers, but the biphenyl core contributes most significantly. [41] Fig. 4a shows an image for the pure liquid crystal 5CB at x = 0 wt-%. It is seen that the domain walls are mostly, straight. The slight degree of domain wall bowing — randomly concave or convex — is typical even for a purely achiral LC, and is due to surface imperfections and the filling process. Fig.'s 4b-f show images for the liquid crystal with an increasing concentration of capsules. We can visually see the increase in curvature with concentration in these samples. The 0 and 0.11 wt-% (Fig.'s 4a,b) samples both exhibit relatively straight lines, and curve fitting confirmed that both samples have inconsistent sense of curvature of the domain walls, with several arcs bowing outward from the "minority" region. This is not unreasonable given the small amount of chiral induction that would occur in the 0.11 wt-% sample and is expected for pure 5CB. For the 0.21 wt-% and 0.32 wt-% samples (Fig.'s 4c,d), the curvature becomes obvious and consistent. The disclination lines bow into the minority regions for all cells with 0.21 wt-% and higher concentration. Finally, the curvature continues to grow, as expected, for the 0.42 and 0.52 wt-% cells (Fig.'s 4e,f).

From these images, we can also note the increasing effects of capsule aggregation in the cells as concentration increases. For the pure 5CB sample the image is very clean, with very few bright spots aside from the disclination lines. This immediately changes once the capsules are introduced (the 0.11 wt-% sample, Fig. 4b). At 0.42 wt-% the aggregations become larger and at 0.52 wt-% some of the aggregations appear to be as much as half the size of the small majority handedness domain within the minority domain. This increasing aggregation suggests that the domain wall curvature measured at a given concentration represents a lower limit for the curvature that would be present if aggregation did not occur.

We examined the deracemization of the liquid crystal in the presence of the capsules, but where the capsules coated with the surfactant Agrimer® AL-22. Here we found that the capsules' surfactant coating prevents close proximity between the chiral surface of the capsules and the surrounding liquid crystal, keeping the two sufficiently far apart to reduce significantly the chiral deracemization.[35] Physical blockage of chiral induction in a liquid crystal by a chiral surface has been demonstrated in the past.[36] The surfactant was mixed in toluene with the capsules before adding liquid crystal with the purpose of functionalizing the outer shell of the capsules to prevent aggregation. These coated capsules were added to 5CB in concentrations of 0.30 and 0.56 wt-%, then placed in a cell with the Raynes geometry. The images showed no sign of chiral induction — within error, there was zero net curvature of the domain walls. Thus, obstruction of the capsules' chiral moiety from the liquid crystal renders the capsules chirally inert, and no systematic chiral effect is observed in the Raynes' geometry.

Let us now turn to the curvature analysis. At least fifteen domain wall segments, generally with an arc-length less than 100 pixels, were selected randomly for each image. Fig. 5 shows the selections made for the x = 0.32 wt-% sample. Fig. 6 shows a plot of the average curvature C *vs.* capsule concentration x. The error bars represent the statistical variation of the curvature values obtained from each of the chosen segments at a given concentration. The error bars are due to several factors, including differences in the local concentration and aggregation of the capsules in each sample, as well as the fitting procedure for an interface that actually is represented by a curve that has a nonzero width of at least one pixel. Nevertheless, the most important observation is that, despite the large spread in curvature at each concentration, there is a general

tendency for C to increase with x, thus indicating the ability of the chiral shells to partially deracemize the surrounding liquid crystal. This is the principal result of this work, *viz.,* that the capsules chiral shell can induce chirality *via* conformational deracemization in the surrounding medium.

Should we expect a linear variation of C vs. x, at least for small concentrations? Ideally, the answer is yes, although there are a number of mitigating factors. It is clear from Fig. 4 that the capsules form aggregates at higher concentrations, at least aggregates that are sufficiently large to be visible. To be sure, there also are aggregates, likely at all concentrations, which are sub-wavelength-of-light in size, and are not visible in these images. Unlike a uniform dispersion of a molecular chiral dopant that is soluble in the liquid crystal, the larger capsule colloids will deracemize the liquid crystal only at the exposed capsule surface. But as the mean spacing between even non-aggregated particles is large, *i.e.,* of order the capsule diameter × (volume fraction)$^{-1/3}$, or approximately 1 to 2 μm for capsule diameters ~ 200 nm at $x \sim 0.5$ wt-%, the chiral induction effect tends to be slightly grainy, resulting in a domain wall curvature that can vary from point to point along the wall. This undesirable effect becomes more pronounced with aggregation, as the net surface area of the chiral aggregates exposed to the liquid crystal is reduced on aggregation. One result of the graininess is the increase in the distribution of fitted radii of curvature, especially at higher concentrations.

An additional consideration comes from imperfections in the surface alignment layer, including the presence of small particulate matter. These imperfections can result in local pinning or modification of domain walls, and thus give rise to nonlinear C vs. x behavior, and even local nonzero curvature for the pure (undoped) 5CB mixture. Finally, we note that the sizes of the minority domains, *i.e.,* the closed regions having the "wrong" handedness, become smaller as the capsule concentration x increases. This is at it should be, as domain walls are mobile and the system will adjust to its global energy minimum. For $x = 0.52$ wt-%, however, the minority domains become quite small. Thus the arc lengths of the domain walls become quite short, down to 20 to 30 pixels. This presents a challenge: fitting a circle to a tiny arc. As a result, we believe that the apparent large average curvature C at $x = 0.52$ wt-% is, in part, an artifact of this fitting.

In conclusion, we have presented a method for preparing chiral nanocapsules with chiral shells. The method is based on nanoemulsification of isocyanate monomers dissolved in organic solvent followed by the addition of chiral diamines to initiate interfacial polymerization and form chiral nanocapsules. These capsules have shown successful induction of deracemization in a surrounding liquid crystal, as measured by the Raynes technique. We believe the results obtained in this work open new avenues in the research of chiral materials and offer the possibility of novel applications of chiral polymeric nanocapsules in many fields, including as chiral separations, asymmetric catalysis and enantioselective release of racemic actives.

Acknowledgments: We thank Raymond Adkins (CWRU) for his assistance with the wall detection and curve fitting and Prof. Robert Lemieux of the University of Waterloo for useful discussions. This work was supported by grant number 2014034 from the US-Israel Binational Science Foundation and from the National Science Foundation's Condensed Matter Physics Program under grant DMR-1505389. CR is grateful to the Lady Davis Trust for support during his stay at the Hebrew University of Jerusalem. We thank Dr. Yael Levi-Kalisman (The Hebrew University Center for Nanoscience and Nanotechnology) for the cryo-TEM measurements.

References

(1) Eliel, E. L.; Wilen, S. H. *Stereochemistry of Organic Compounds*; John Wiley and Sons: New York, 1994.
(2) Berardi, R.; Kuball, H.-G.; Memmer, R.; Zannoni, C. Chiral induction in nematics. A computer simulation study. *J. Chem. Soc., Faraday Trans.* **1998**, *94*, 1229-1234.
(3) MacQuarrie, S.; Thompson, M. P.; Blanc, A.; Mosey, N. J.; Lemieux, R. P.; Crudden, C. M. Chiral periodic mesoporous organosilicates based on axially chiral monomers: transmission of chirality in the solid state. *J. Am. Chem. Soc.* **2008**, *130*, 14099-14101.
(4) Basu, R.; Chen, C.-L.; Rosenblatt, C. Carbon nanotube-induced macroscopic helical twist in an achiral nematic liquid crystal. *J. Appl. Phys.* **2011**, *109*, 083518/1-083518/4.
(5) Jayalakshmi, V.; Wood, T.; Basu, R.; Du, J.; Blackburn, T.; Rosenblatt, C.; Crudden, C. M.; Lemieux, R. P. Probing the pore structure of a chiral periodic mesoporous organosilica using liquid crystals. *J. Mater. Chem.* **2012**, *22*, 15255-15261.

(6) Zaera, F. Chirality in adsorption on solid surfaces. *Chem. Soc. Rev.* **2017**, *46*, 7374-7398.
(7) Ma, W.; Xu, L.; de Moura, A. F.; Wu, X.; Kuang, H.; Xu, C.; Kotov, N. A. Chiral inorganic nanostructures. *Chem. Rev.* **2017**, *117*, 8041-8093.
(8) Wang, Y.; Xu, J.; Wang, Y.; Chen, H. Emerging chirality in nanoscience. *Chem. Soc. Rev.* **2013**, *42*, 2930-2962.
(9) Song, C.; Liu, X.; Liu, D.; Ren, C.; Yang, W.; Deng, J. Optically active particles of chiral polymers. *Macromol. Rapid Commun.* **2013**, *34*, 1426-1445.
(10) Yoon, M.; Srirambalaji, R.; Kim, K. Homochiral metal-organic frameworks for asymmetric heterogeneous catalysis. *Chem. Rev.* **2012**, *112*, 1196-1231.
(11) Morris, R. E.; Bu, X. Induction of chiral porous solids containing only achiral building blocks. *Nat. Chem.* **2010**, *2*, 353-361.
(12) Raval, R. Chiral expression from molecular assemblies at metal surfaces: insights from surface science techniques. *Chem. Soc. Rev.* **2009**, *38*, 707-721.
(13) Mastai, Y. Enantioselective crystallization on nanochiral surfaces. *Chem. Soc. Rev.* **2009**, *38*, 772-780.
(14) Harris, K. D. M.; Thomas, S. J. M. Selected thoughts on chiral crystals, chiral surfaces, and asymmetric heterogeneous catalysis. *ChemCatChem* **2009**, *1*, 223-231.
(15) Marx, S.; Avnir, D. The induction of chirality in sol-gel materials. *Acc. Chem. Res.* **2007**, *40*, 768-776.
(16) Jyothi, N. V. N.; Prasanna, P. M.; Sakarkar, S. N.; Prabha, K. S.; Ramaiah, P. S.; Srawan, G. Y. Microencapsulation techniques, factors influencing encapsulation efficiency. *J. Microencapsulation* **2010**, *27*, 187-197.
(17) Dubey, R.; Shami, T. C.; Rao, K. U. B. Microencapsulation technology and applications. *Def. Sci. J.* **2009**, *59*, 82-95.
(18) Lensen, D.; Vriezema, D. M.; van Hest, J. C. M. Polymeric microcapsules for synthetic applications. *Macromol. Biosci.* **2008**, *8*, 991-1005.
(19) Yow, H. N.; Routh, A. F. Formation of liquid core-polymer shell microcapsules. *Soft Matter* **2006**, *2*, 940-949.
(20) Perignon, C.; Ongmayeb, G.; Neufeld, R.; Frere, Y.; Poncelet, D. Microencapsulation by interfacial polymerisation: membrane formation and structure. *J. Microencapsulation* **2015**, *32*, 1-15.
(21) Zhang, Y.; Rochefort, D. Characterisation and applications of microcapsules obtained by interfacial polycondensation. *J. Microencapsulation* **2012**, *29*, 636-649.
(22) Jadhav, K. T.; Babu, P. V. V. A review on interfacial polycondensation technique: types, applications and effect of various parameters. *Int. J. Biotechnol., Chem. Environ. Eng.* **2012**, *1*, 49-55.
(23) Potts, A.; Zhang, W.; Bagnall, D. M. A new polarimeter based on optical non-reciprocity in gratings with two-dimensional chirality. *Appl. Phys. B: Lasers Opt.* **2010**, *99*, 679-693.
(24) Walba, D. M.; Clark, N. A. Methods for determination of enantiomeric excess of chiral compounds using liquid crystals. US Patent 7374948, 2008.
(25) Huang, Y.; Zhou, Y.; Wu, S.-T. Spatially tunable laser emission in dye-doped photonic liquid crystals. *Appl. Phys. Lett.* **2006**, *88*, 011107/1-011107/3.
(26) Strangi, G.; Barna, V.; Caputo, R.; De Luca, A.; Versace, C.; Scaramuzza, N.; Umeton, C.; Bartolino, R.; Price, G. N. Color-tunable organic microcavity laser array using distributed feedback. *Phys. Rev. Lett.* **2005**, *94*, 063903/1-063903/4.

(27) Komitov, L.; Helgee, B.; Felix, J.; Matharu, A. Electrically commanded surfaces for nematic liquid crystal displays. *Appl. Phys. Lett.* **2005**, *86*, 023502/1-023502/3.
(28) Cao, W.; Munoz, A.; Palffy-Muhoray, P.; Taheri, B. Lasing in a three-dimensional photonic crystal of the liquid crystal blue phase II. *Nat. Mater.* **2002**, *1*, 111-113.
(29) Kopp, V. I.; Fan, B.; Vithana, H. K. M.; Genack, A. Z. Low-threshold lasing at the edge of a photonic stop band in cholesteric liquid crystals. *Opt. Lett.* **1998**, *23*, 1707-1709.
(30) Moore, D. E.; Meeker, K.; Ellis, A. B. Detection of chiral analytes through adduct formation with chiral films coated onto emissive cadmium selenide substrates. *J. Am. Chem. Soc.* **1996**, *118*, 12997-13001.
(31) Kempe, M. Antibody-mimicking polymers as chiral stationary phases in HPLC. *Anal. Chem.* **1996**, *68*, 1948-53.
(32) Yablonovitch, E. Inhibited spontaneous emission in solid-state physics and electronics. *Phys. Rev. Lett.* **1987**, *58*, 2059-62.
(33) John, S. Strong localization of photons in certain disordered dielectric superlattices. *Phys. Rev. Lett.* **1987**, *58*, 2486-9.
(34) Friedel, G. The mesomorphic states of matter. *Ann. phys.* **1922**, *18*, 273-474.
(35) Pieraccini, S.; Masiero, S.; Ferrarini, A.; Piero Spada, G. Chirality transfer across length-scales in nematic liquid crystals: fundamentals and applications. *Chem. Soc. Rev.* **2011**, *40*, 258-271.
(36) Ferrarini, A.; Moro, G. J.; Nordio, P. L. Simple molecular model for induced cholesteric phases. *Phys. Rev. E: Stat. Phys., Plasmas, Fluids, Relat. Interdiscip. Top.* **1996**, *53*, 681-688.
(37) Memmer, R.; Kuball, H. G.; Schoenhofer, A. Computer simulation of chiral liquid crystal phases. III. A cholesteric phase formed by chiral Gay-Berne atropisomers. *Mol. Phys.* **1996**, *89*, 1633-1649.
(38) Canny, J. A computational approach to edge detection. *IEEE Trans Pattern Anal Mach Intell* **1986**, *8*, 679-98.
(39) Raynes, E. P. The use of bowed reverse twist disclination lines for the measurement of long pitch lengths in chiral nematic liquid crystals. *Liq. Cryst.* **2006**, *33*, 1215-1218.
(40) DeGennes, P. G.; Prost, J. *The Physics of Liquid Crystals*; Oxford University Press: New York, 1994.
(41) Greco, C.; Ferrarini, A. Electroclinic effect in nematic liquid crystals: the role of molecular and environmental chirality. *Phys. Rev. E: Stat., Nonlinear, Soft Matter Phys.* **2013**, *87*, 060501/1-060501/4.

Scheme and Figures

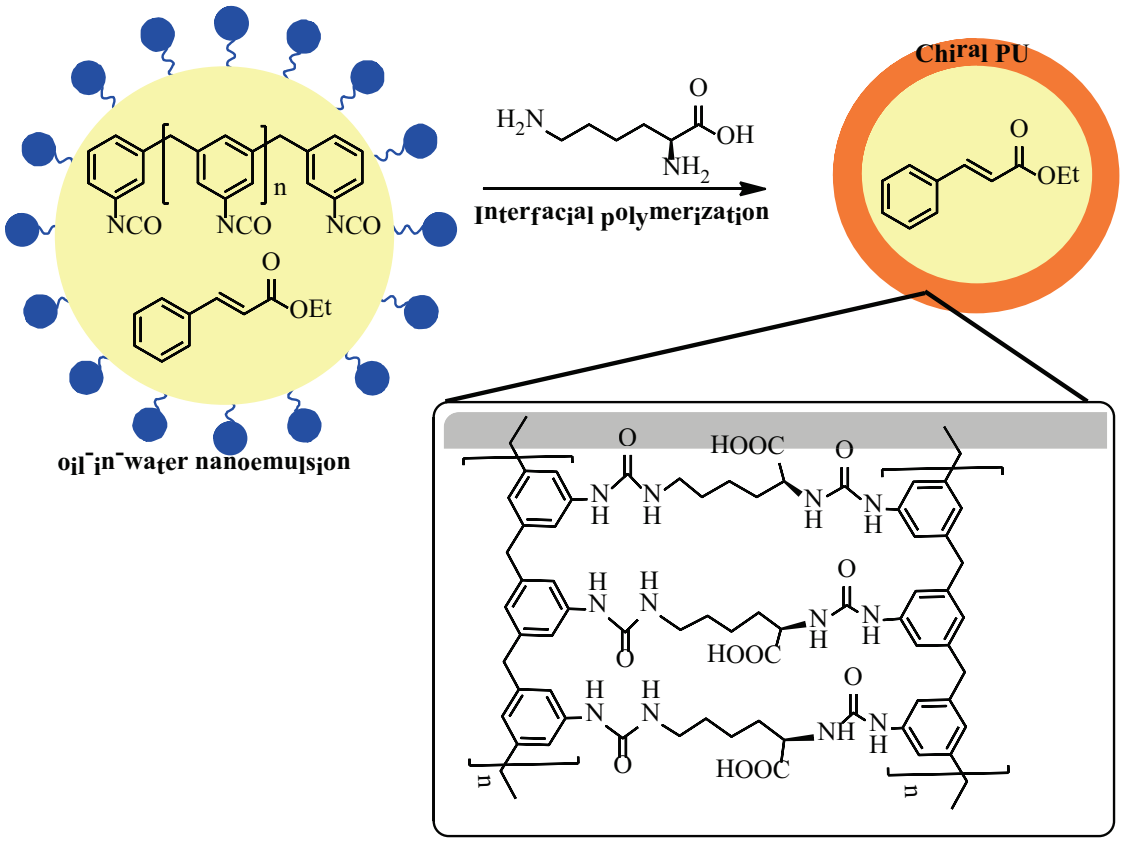

Scheme 1. Preparation of chiral polyurea nanocapsules.

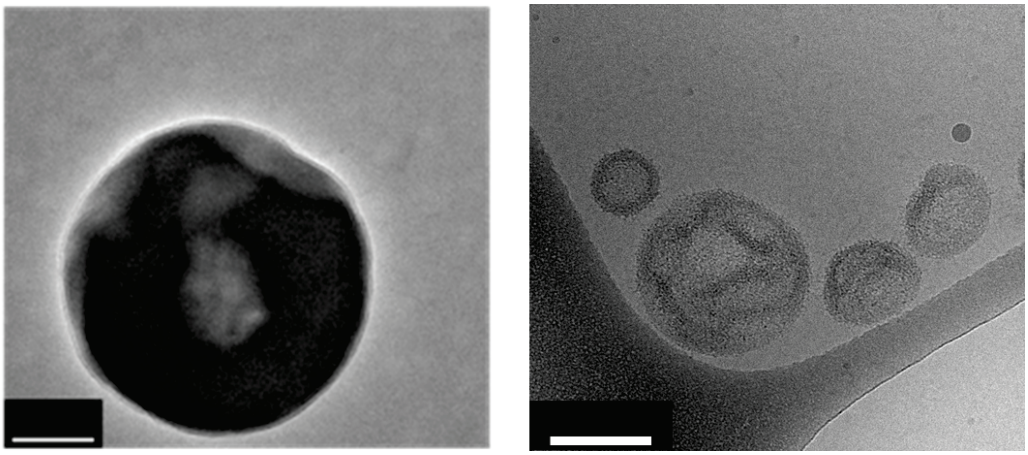

Figure 1. TEM image (left, scale bar = 100 nm) and cryo-TEM image (right, scale bar = 500 nm) of the chiral polyurea nanocapsules.

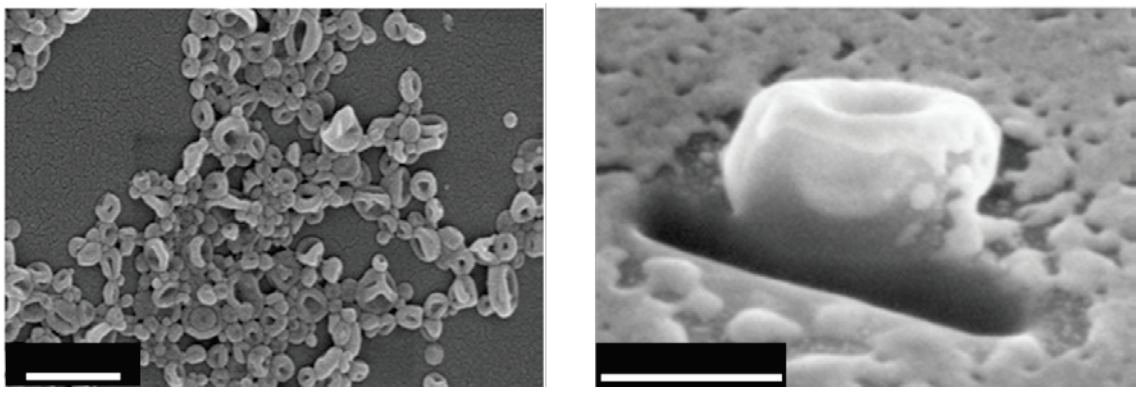

Figure 2. The hollow nature of these capsules is also revealed by their collapse under SEM conditions (left, scale bar = 500 nm) and SEM after dissection with focused ion beam (right, scale bar = 100 nm).

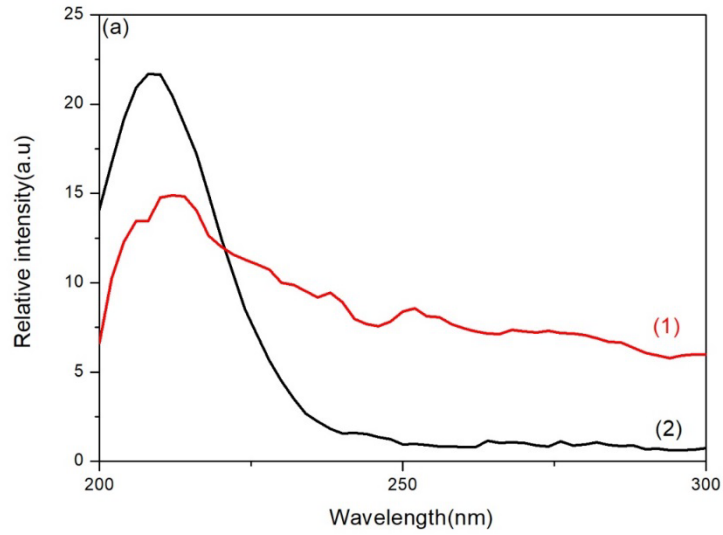
(a)
Relative intensity(a.u)
Wavelength(nm)
(1)
(2)
0
5
10
15
20
25
200
250
300

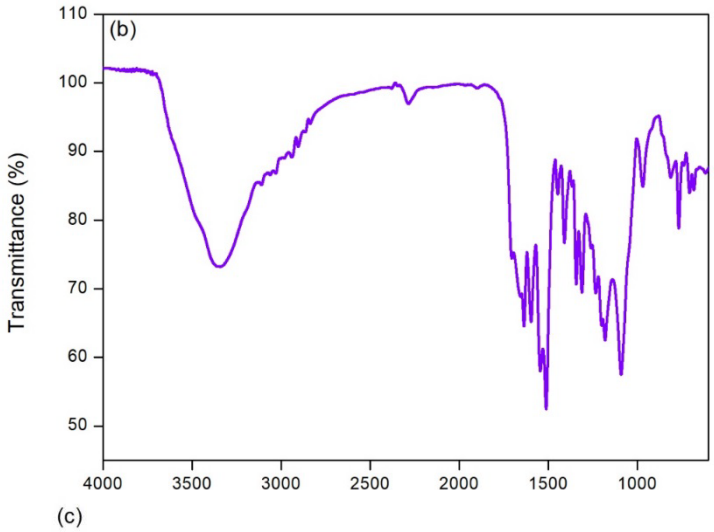
(b)
Transmittance (%)
50
60
70
80
90
100
110
4000
3500
3000
2500
2000
1500
1000

(c)

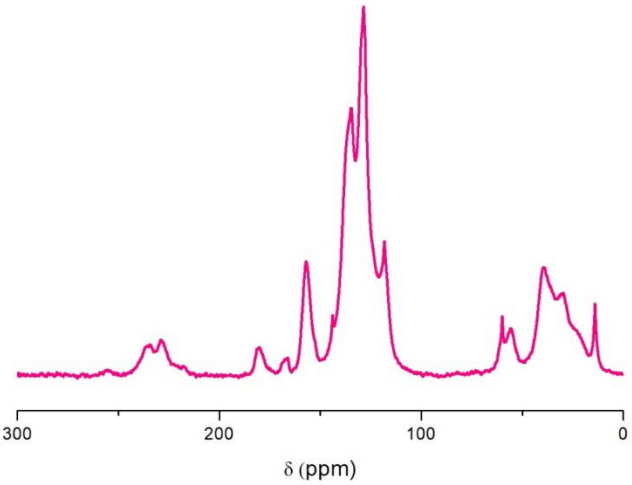
300
200
100
0
δ (ppm)

Figure 3. Spectral analysis and structural confimation of the polymeric shell composition. (a) Circular dichroism spectrum, (1) chiral polyurea nanocapsules, (2) L-lysine**.** (b) IR spectrum with some indicative peaks and no trace of the isocyanate group. (c) ^{13}C CP-MAS NMR spectrum. See text for peaks assignments.

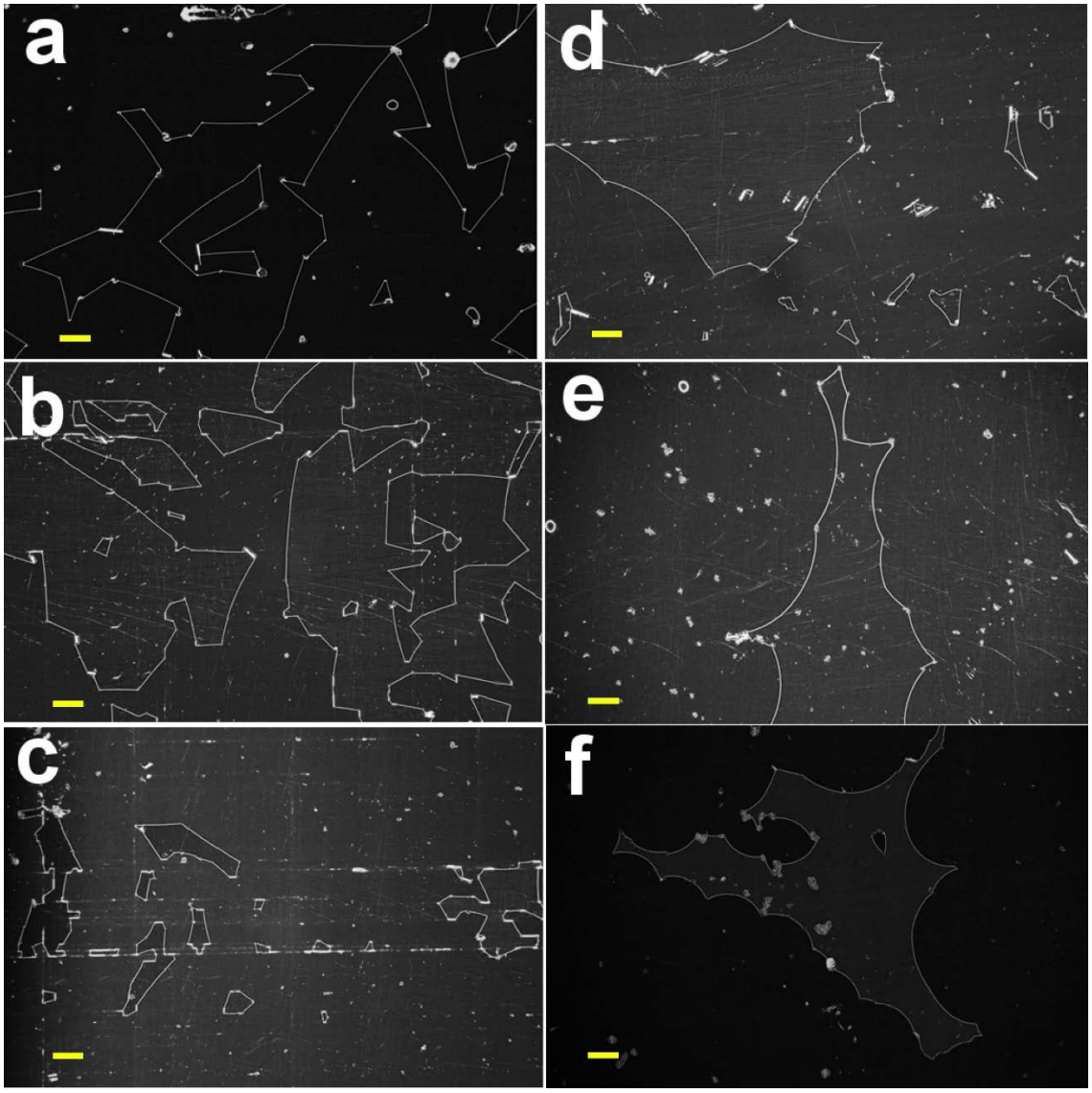

Figure 4. Polarizing microscope images showing domain walls separating the right- and left-handed twist domains. Images *a* through *f* correspond to concentrations of x = 0, 0.11, 0.21, 0.32, 0.42, and 0.52 wt-%. Scale bar is 100 micrometer.

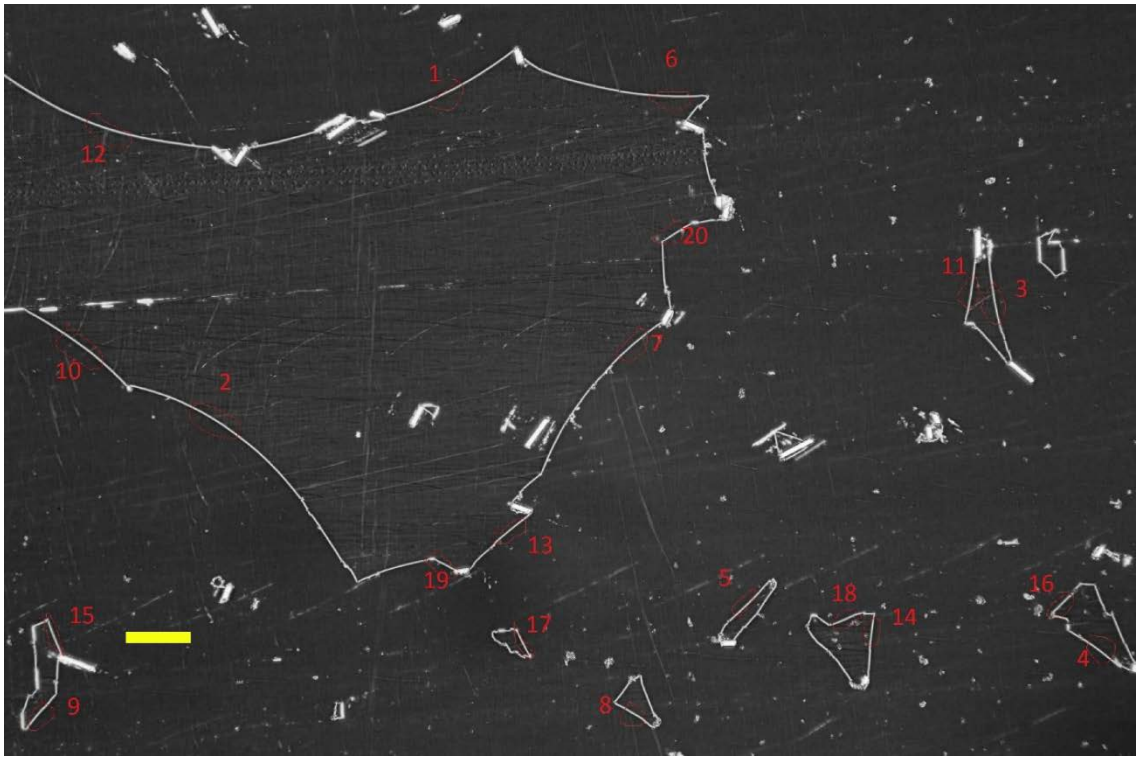

Figure 5. Twenty regions selected for quantitative curvature analysis for the x = 0.32 wt-% sample. Scale bar is 100 micrometer.

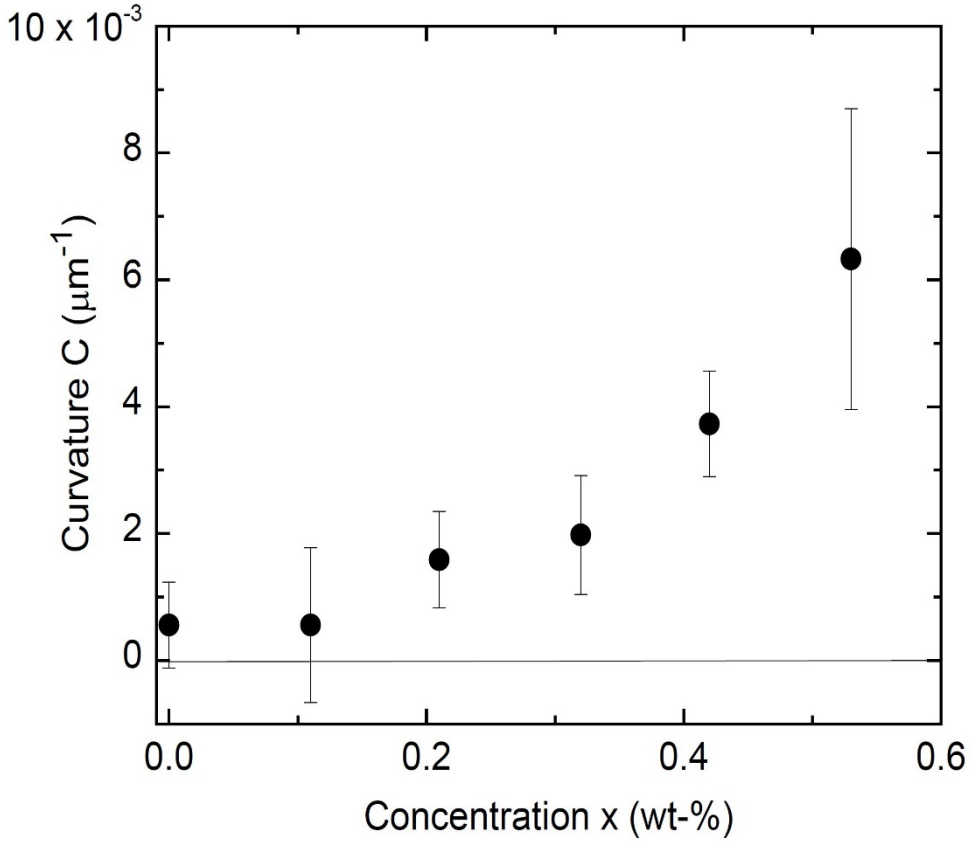

Figure 6. Average curvature *vs.* prepared concentration of capsules in the liquid crystal.